ISPRS Journal of Photogrammetry and Remote Sensing 165 (2020) 140–151

Contents lists available at ScienceDirect

ISPRS Journal of Photogrammetry and Remote Sensing

journal homepage: www.elsevier.com/locate/isprsjprs

Mapping $PM_{2.5}$ concentration at a sub-km level resolution: A dual-scale retrieval approach

Qianqian Yang[a], Qiangqiang Yuan[a,b,*], Linwei Yue[c], Tongwen Li[d,*], Huanfeng Shen[d], Liangpei Zhang[e]

[a] School of Geodesy and Geomatics, Wuhan University, Wuhan, Hubei 430079, China
[b] Key Laboratory of Geospace Environment and Geodesy, Ministry of Education, Wuhan University, Wuhan 430079, Hubei, China
[c] School of Geography and Information Engineering, China University of Geosciences, Wuhan, Hubei 430074, China
[d] School of Resource and Environmental Sciences, Wuhan University, Wuhan, Hubei 430079, China
[e] State Key Laboratory of Information Engineering, Survey Mapping and Remote Sensing, Wuhan University, Wuhan, Hubei 430079, China

ARTICLE INFO

Keywords:
$PM_{2.5}$
Retrieval
Aerosol optical depth
High resolution
Dual-scale
Scale difference

ABSTRACT

Satellite-based retrieval has become a popular $PM_{2.5}$ monitoring method. To improve the retrieval performance, multiple variables are usually introduced as auxiliary variables, in addition to aerosol optical depth (AOD). The different kinds of variables are usually at different resolutions, varying from sub-kilometer to dozens of kilometers. Generally speaking, when undertaking the retrieval, the variables at different resolutions are resampled to the same resolution as the AOD product to ensure scale consistency (single-scale retrieval). However, a drawback of doing this is that the information contained within the different resolutions (scales) is discarded. To fully utilize the information contained in the different scales, a dual-scale retrieval approach is proposed in this paper. In the first stage, the variables which influence $PM_{2.5}$ concentration at a large scale are used for $PM_{2.5}$ retrieval at a coarse resolution. Then, in the second stage, the variables which affect $PM_{2.5}$ distribution at a finer scale are used for the further $PM_{2.5}$ retrieval at a high resolution (sub-km level resolution), with the retrieved low-resolution $PM_{2.5}$ from the first stage also acting as input. In this study, four different regression models were adopted to test the performance of the dual-scale retrieval approach at both daily and annual scales: multiple linear regression (MLR), geographically weighted regression (GWR), random forest (RF), and the generalized regression neural network (GRNN). Compared with the traditional single-scale retrieval approach, the proposed dual-scale retrieval approach can achieve $PM_{2.5}$ mapping at a finer resolution and with a higher accuracy. Dual-scale retrieval can utilize the information contained in different scales, thus achieving an improvement in both resolution and retrieval accuracy. The proposed approach has the potential to be used for the generation of quantitative remote sensing products in various fields, and will promote the quality improvement of these quantitative remote sensing products.

1. Introduction

Fine particulate matter with an aerodynamic diameter of less than 2.5 μm ($PM_{2.5}$) poses a great threat to the ecological environment and public health (Cao et al., 2016; Chen et al., 2019; Ho et al., 2018; Lelieveld et al., 2015). As a result, ground environmental monitoring sites have been built worldwide for the measuring of $PM_{2.5}$ concentration. However, site-based measurement cannot achieve large-scale monitoring with continuous spatial coverage (Gupta et al., 2006; van Donkelaar et al., 2010). As a supplement, satellite-based remote sensing retrieval has become popular methods for $PM_{2.5}$ monitoring in recent years (de Hoogh et al., 2018; Hu et al., 2014; Stafoggia et al., 2019; van Donkelaar et al., 2015).

The basic satellite product required for $PM_{2.5}$ retrieval is the aerosol optical depth (AOD), which usually holds a spatial resolution at the kilometer level; for instance, 10 km (MOD04), 6 km (VIIRS EDR), 3 km (MOD04_3K), 1 km (MAIAC), 750 m (VIIRS IP) (Ceca et al., 2018; Jackson et al., 2013; Liu et al., 2019; Wang et al., 2019a; Wei et al., 2019; Xiao et al., 2017). In addition to AOD, other variables such as meteorological and topographical factors have also been included as auxiliary variables, to promote the performance of the retrieval model (Bi et al., 2019; Chen et al., 2018; Tai et al., 2010). Meteorological variables are usually at a coarse resolution (dozens of kilometers level), while topographical data (such as digital elevation models (DEMs) and

* Corresponding authors at: School of Geodesy and Geomatics, Wuhan University, Wuhan, Hubei 430079, China (Q. Yuan).
E-mail addresses: qqyuan@sgg.whu.edu.cn (Q. Yuan), litw@whu.edu.cn (T. Li).

https://doi.org/10.1016/j.isprsjprs.2020.05.018
Received 14 October 2019; Received in revised form 19 May 2020; Accepted 22 May 2020
Available online 30 May 2020

land-cover data) are usually at a fine resolution (sub-kilometer level). In fact, the resolution of the variables used for $PM_{2.5}$ retrieval often varies over a wide range, from sub-kilometer to dozens of kilometers. When establishing the retrieval model, to keep the scale consistency, the input variables are usually resampled to the same resolution as the AOD product (which we call "single-scale retrieval") (Boys et al., 2014; Li et al., 2017a). To be more specific, the variables at a higher resolution than AOD product are upscaled, and the variables at a lower resolution than AOD product are downscaled, both to the resolution of AOD product. However, the variables at different resolutions often contain information at different levels of detail. Simple resampling to the same resolution as AOD product may bring about information loss, especially the loss of detail information at the sub-kilometer level, and therefore make the final product at a relatively coarse resolution. As another option, we may also resample all the data to the finest resolution of all the input data, for example, to the resolution of topographical variables in $PM_{2.5}$ retrieval problem. However, this way can introduce large uncertainties, and the model performance can be worse (refer to supplementary material Text 5). Hence, studying how to consider the resolution differences of input variables into the retrieval model and make better use of the detail information contained in the fine-scale variables can be of vital importance for high-resolution $PM_{2.5}$ mapping.

In a recent study by Peng et al. (2017), they claimed that the dominant physical controls on the spatial variability of soil moisture can be a function of scale, as shown in Fig. S1. This means that different factors may dominate the spatial variations of soil moisture at different scales. For $PM_{2.5}$ concentration, this may also apply. For example, meteorological factors usually dominate the spatial variation of $PM_{2.5}$ at a large scale, and topographical factors usually dominate at a finer scale. Based on this principle, we proposed the dual-scale retrieval approach, which retrieves $PM_{2.5}$ concentration through two stages. In the first stage, $PM_{2.5}$ concentration at a coarse resolution is retrieved with the variables which mainly dominate the spatial variation of $PM_{2.5}$ at a large scale. Then, in the second stage, the retrieved low-resolution $PM_{2.5}$ concentration, together with the variables which dominate the fine-scale spatial variations of $PM_{2.5}$, are used for the retrieval at a fine scale. In this way, the predictors are all making predictions at the scale they dominate rather than mix-up, thus have the potential to show a higher predicting ability. The two-stage dual-scale retrieval method considers the difference of information embodied in the different scales and therefore has the potential to bring improvement in both product resolution and model performance.

In this study, we selected two linear retrieval models, i.e., multiple linear regression (MLR) (Bottenberg and Ward, 1963; Xu et al., 2018) and geographically weighted regression (GWR) (Brunsdon et al., 1996; Jiang et al., 2017), and two machine learning (ML) based nonlinear models, i.e., random forest (RF) (Breiman, 2001; Hu et al., 2017; Huang et al., 2018) and the generalized regression neural network (GRNN) (Cigizoglu and Alp, 2006; Li et al., 2017b), to test the performance of the dual-scale retrieval method. For a fair comparison with the single-scale retrieval approach, we used the same models in the two stages. Nine meteorological variables and the Moderate Resolution Imaging Spectroradiometer (MODIS) AOD product at a 0.1° resolution were used for the first-scale retrieval. DEM and land-cover data were then used for the second-scale estimation. The dual-scale retrieval model was then built for China in 2015 at both daily and annual scales. Ten-fold cross-validation and dense-point cross-validation were used for the quantitative evaluation of the model performance. After the model building, we mapped the $PM_{2.5}$ concentration in 2015 for several typical cities in China at the $0.003^\circ \times 0.003^\circ$ resolution, and the spatial distribution of the $PM_{2.5}$ concentration was analyzed at a fine scale. The quantitative evaluation and mapping results showed that the dual-scale method can not only achieve a better model performance with a higher retrieval accuracy, but can also output the $PM_{2.5}$ product with a higher resolution and capture the fine-scale spatial variations better than the traditional single-scale retrieval approach.

The rest of this paper is organized as follows. In Section 2, we introduce the data sources and the methodology, and provide a flow chart of the study design. The experimental results are provided in Section 3. Then, in section 4, we make a discussion about the results and state the limitations and future work. Finally, we make a summary of our work in Section 5.

2. Data and method

2.1. Study area

China is a large country with dense population and broad territory. The rapid economic development in recent decades has resulted in serious pollution in China (Li et al., 2016; Ma et al., 2016). Since 2013, multiple environmental monitoring stations have been built in China for the monitoring of air quality, providing a foundation for air pollution research. Up to 2015, these stations covered 368 cities in China. In this study, $PM_{2.5}$ data from these stations were used as output for the model training. As for the retrieval phase, we chose five typical cities in China for the mapping of $PM_{2.5}$ concentration. The selected cities were Beijing, Wuhan, Shanghai, Guangzhou, and Chengdu, which are located in the northern, central, eastern, southern, and western parts of China, respectively. Beijing, the capital city of China, locates in the Northern China Plain. Beijing is marked by its flatness and arid climate. There are only three hills to be found in the city limits, and mountains surround the capital on three sides. Affected by the rapid urbanization in recent years and the unfavorable topographic conditions, $PM_{2.5}$ pollution has become an urgent problem for Beijing (Guo et al., 2017). Wuhan is the largest city in Central China, with a dense population of 11,081,000. With the Yangtze River running through the city, Wuhan has a humid climate, and the dominant terrain is plain. Impacted by the heavy industry production, $PM_{2.5}$ pollution is also a serious problem for Wuhan (Zhang et al., 2018). Shanghai, which is the largest economic and transportation center in China, locates in the Yangtze River Delta in East China and sits on the south edge of the mouth of the Yangtze in the middle portion of the eastern Chinese coast. As the cradle of China's modern industry, Shanghai undertakes much of the industrial production in China. When combined with the rapid economic development, $PM_{2.5}$ concentration has been increasing in recent decades (He et al., 2018). Guangzhou is the central city of South China and is located in the flourishing Pearl River Delta region. With the Tropic of Cancer passing north of the city and the Pearl River flowing through the city, Guangzhou enjoys favorable weather, which is warm and humid. When compared with the aforementioned cities, the $PM_{2.5}$ pollution in Guangzhou is less serious (Yang et al., 2017b). Chengdu is located at the western edge of the Sichuan Basin and sits on the Chengdu Plain. The dominant terrain in this area is plains, but the city is surrounded by high mountains. Chengdu has a similar climate to Wuhan, i.e., adequate precipitation, humid, and mild. Chengdu is also one of the most important economic centers and transportation/communication hubs in Western China. The unique topography also makes the air pollution situation in Chengdu unique (Ning et al., 2018). The selected cities cover different topographies, climates, and pollution degrees, allowing a comprehensive assessment of the model performance. The locations and the topographies of these cities are displayed in Fig. 1.

2.2. Datasets

2.2.1. Ground site $PM_{2.5}$ data

The ground-based $PM_{2.5}$ concentration data from the environmental monitoring stations were provided by the Ministry of Ecology and Environment of the People's Republic of China (http://www.mee.gov.cn/). Hourly $PM_{2.5}$ concentration data for more than 1400 sites in 2015 were collected. After outlier filtering, the hourly $PM_{2.5}$ data were averaged to daily and annual data for the daily and annual modeling, respectively. The distribution of the monitoring sites is shown in Fig. 1.

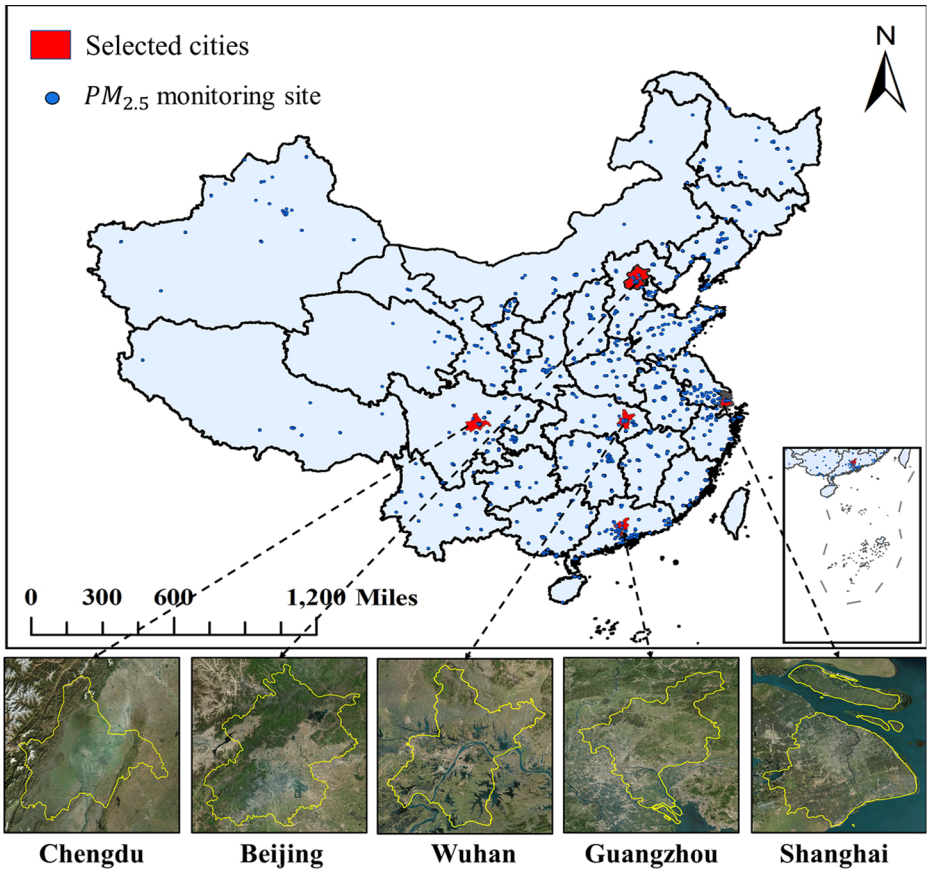

Fig. 1. Study area. The map shows the distribution of $PM_{2.5}$ monitoring sites (blue points) and the locations of the five selected cities (red polygons). The satellite images show the topography of the five cities, while the yellow lines are the administrative boundaries of these cities. The images were provided by ArcGIS Online World Imagery.

2.2.2. AOD data

AOD represents the vertical integral of the aerosol extinction coefficient on the atmospheric column (Chung, 2012). It can measure the particles in the air indirectly and has thus been widely used for retrieving $PM_{2.5}$ concentration (Chen et al., 2018; Guo et al., 2009; Yang et al., 2018). The satellite AOD product used in this study was provided by the Atmosphere Archive and Distribution System (LAADS) Distributed Active Archive Center (DAAC) of NASA (https://ladsweb.modaps.eosdis.nasa.gov/). The 10 km MODIS Collection 6 Level 2 daily AOD data (MOD04_L2) retrieved from Dark Target algorithms were used in this study (Levy et al., 2013; Levy et al., 2007; Wang et al., 2019b). To ensure the data quality, only data with the best quality (Quality flag = 3) was used.

2.2.3. Meteorological data

Many researchers have proved that meteorological conditions can have a significant impact on $PM_{2.5}$ concentration (Chen et al., 2017; Tai et al., 2010; Yang et al., 2017a), and the introduction of meteorological factors can improve the retrieval accuracy (Tian and Chen, 2010). In this study, several commonly used meteorological variables were obtained from the Modern-Era Retrospective Analysis for Research and Applications, version 2 (MERRA-2) dataset with a resolution of 0.5° × 2/3° (daily) and considered in the retrieval model: 2-m air temperature (TMP), surface pressure (PS), 2-m specific humidity (SH), 2-m eastward wind speed (UWS), 2-m northward wind speed (VWS), lifting condensation level (LCL), vertical pressure velocity at 500 hPa (OME), total precipitation (PR), and planetary boundary layer height (PBLH).

2.2.4. Topographical data

Although not used as much as meteorological factors in $PM_{2.5}$ retrieval, topographical factors can also affect $PM_{2.5}$ pollution, and can help to improve the performance of the retrieval model (Beloconi et al., 2016; Jung et al., 2018; Wang et al., 2017). Therefore, the topographical factors including land cover (LC) and elevation (DEM) were also considered in this study. The land-cover product was provided by the European Space Agency (ESA) Climate Change Initiative (CCI) (http://maps.elie.ucl.ac.be/CCI/viewer/index.php), with a spatial resolution of 300 m. The original product is classified into 22 classes, and some classes were not found in the study area. Therefore, in our study, the product was integrated into eight classes, i.e., farmland, woodland, grassland, sparse vegetation, bare land, urban area, water body, and snow and ice. The 30-m elevation data were obtained from the Global Seamless DEM Based on Multi-Source Data Fusion product (GSDEM-30) (Yue et al., 2015; Yue et al., 2017), which can be downloaded from http://sendimage.whu.edu.cn/res/DEM_share/. For consistency with the land-cover data, the 30-m DEM data were resampled to 300 m through pixel aggregate method. Therefore, the used topographical data, i.e., the DEM and land-cover data, were all at a 300-m resolution. To unify the coordinate system (the AOD and meteorological data were in a geographic coordinate system and the topographical data were in a projected coordinate system), the projected coordinate system was reprojected into the World Geodetic System 1984 (WGS84) geographic coordinate system, and were then resampled into 0.003° (10 km ~ = 0.1°)°.

A summary of variables used for $PM_{2.5}$ retrieval and more details about data preprocessing in this study can be found in the Supplementary material (Table S1 and Text 1).

2.3. Methodology

2.3.1. Model development

For a full test of the performance of dual-scale retrieval, we developed the model at both daily and annual scales. Daily $PM_{2.5}$ concentration, AOD, and other auxiliary variables were used for the daily modeling, which can achieve the $PM_{2.5}$ retrieval at the temporal resolution of daily. Then, the annual average values of these data were

used for the annual modeling.

For both modeling scales, the process of the dual-scale retrieval method can be similar, which included two main stages. In the first stage, a low-resolution $PM_{2.5}$ product was retrieved using the AOD and meteorological factors. The meteorological data were resampled to match the AOD grids through bilinear interpolation, and the retrieved $PM_{2.5}$ product was then at the same resolution as the AOD. Considering that $PM_{2.5}$ concentration usually contains strong spatiotemporal autocorrelation (Li et al., 2017a), the longitude and latitude information were input into the model. Specially, for the daily model, the month information was also input. Hence, the process of stage one can be shown as:

$$PM_{2.5\_L} = f(lat, lon, AOD, TMP, PS, SH, UWS, VWS, LCL, OME, PR, PBLH, [month])$$

where $PM_{2.5\_L}$ stands for the retrieved low-resolution $PM_{2.5}$ concentration, and *f()* represents the retrieval models, including MLR, RF, and GRNN models. [ ] means that the variable inside was included in the daily model but not included in the annual model. For GWR model, longitude and latitude information are not used as input but used for calculating the weights in the model, therefore, the process of stage one for GWR is expressed as:

$$PM_{2.5\_L} = f_{GWR}(AOD, TMP, PS, SH, UWS, VWS, LCL, OME, PR, PBLH, [month])$$

In the second stage, the final high-resolution $PM_{2.5}$ product was obtained with the low-resolution $PM_{2.5}$ product produced in the first stage as input. The $PM_{2.5\_L}$ product from stage one was resampled to the resolution of 0.003° using bilinear interpolation and then were input into the second-stage retrieval model together with the 0.003° land-cover and DEM data. At a higher resolution, spatial and temporal information may have a different impact on $PM_{2.5}$ distribution, so the longitude, latitude, and month were introduced into the model again. Besides, considering that the main predictors (topographical data) used in the second stage were all at a temporal resolution of annual and the information about daily variations can be limited, we utilized the temporal autocorrelation of $PM_{2.5}$ and input a temporal term (Li et al., 2017a) into the daily model. The calculation formula of the temporal term can be expressed as:

$$TT_{PM2.5} = \frac{\sum_{i=1}^{n} w_i PM_{2.5,i}}{\sum_{i=1}^{n} w_i} \qquad w_i = \frac{1}{dt_i}$$

where $TT_{PM2.5}$ represents the temporal term, w_i is the weight for $PM_{2.5}$ concentration on day i, dt_i refers to the temporal distance of day i, n is the number of neighboring days used for calculating temporal term and is set to be 10 in this study (Li et al., 2017a). Then, the process of stage two can be simply written as:

$$PM_{2.5\_H} = f(lat, lon, PM_{2.5\_L}, LC, DEM, [month, TT_{PM2.5}])$$

where $PM_{2.5\_H}$ stands for the final high-resolution $PM_{2.5}$ product, *f()* represents the retrieval models including MLR, RF, or GRNN model. [ ] means that the variables inside were included in the daily model but not included in the annual model. Similar to the first stage, in the GWR model, longitude and latitude information were not used as input but used for calculating the weights in the model, and the equation for GWR is written as:

$$PM_{2.5\_H} = f(PM_{2.5\_L}, LC, DEM, [month, TT_{PM2.5}])$$

LC stands for the land cover, which in this study was input in the form of class percentage in a buffer. That is to say, it contained eight variables in total, which represented the proportion of the eight land-cover classes in the buffer. The buffer radius was set as 0.045°, namely 15 pixels after a parameter sensitivity test (refer to supplementary material Text 2).

Taking the daily GWR model as an example, the two stages can be represented as:

(1) Stage one:

$$PM_{2.5\_L,j} = \beta_1(u_j, v_j)AOD_j + \beta_2(u_j, v_j)TMP_j + \beta_3(u_j, v_j)PS_j + \beta_4(u_j, v_j)SH_j + \beta_5(u_j, v_j)UWS_j + \beta_6(u_j, v_j)VWS_j + \beta_7(u_j, v_j)LCL_j + \beta_8(u_j, v_j)OME_j + \beta_9(u_j, v_j)PR_j + \beta_{10}(u_j, v_j)PBLH_j + \beta_{11}(u_j, v_j)month_j + \beta_{12}(u_j, v_j) + \varepsilon_j$$

where $\beta_i(u_j, v_j)$, $i = 1, 2, ...11$ are the regression coefficients at location j for variable i, and $\beta_{12}(u_j, v_j)$ is the intercept, ε_j is the error term.

(2) Stage two:

$$PM_{2.5\_H,j} = \alpha_1(u_j, v_j)PM_{2.5\_L,j} + \alpha_2(u_j, v_j)LC_j + \alpha_3(u_j, v_j)DEM_j + \alpha_4(u_j, v_j)month_j + \alpha_5(u_j, v_j)TT_{PM2.5} + \alpha_6(u_j, v_j) + \varepsilon_j$$

where $\alpha_i(u_j, v_j)$, $i = 1, 2, ...5$ are the regression coefficients at location j for variable i, and $\alpha_6(u_j, v_j)$ is the intercept, ε_j is the error term.

A more detailed introduction to the four different retrieval models (MLR, GWR, RF, and GRNN) and how they are combined with the dual-scale retrieval can be found in the supplementary material Text 3.

For each stage, we first preprocessed the data to obtain data pairs for the model training. The preprocessing procedure included simple gap-filling and data matching. The AOD and DEM data missing in a small spatial range was filled using inverse distance weighting (IDW) interpolation. All the raster data were then matched with the ground environmental stations, according to the longitude and latitude. Secondly, the obtained data pairs were used for training the retrieval model, with $PM_{2.5}$ concentration from the ground sites as the output and the other data as input. The overall workflow is shown in Fig. 2.

2.3.2. Model validation

To validate the performance of the proposed retrieval method, we adopted the sample-based 10-fold cross-validation technique and calculated the coefficient of determination (R^2) for the quantitative indication of the model performance (Li et al., 2017b; Ma et al., 2014). In addition, considering the resolution difference between the single-scale and dual-scale results, we also conducted another validation method, which we call “dense-point cross-validation”. As the final generated product had a higher resolution than the general product from the single-scale retrieval, when several sites were located at the same pixel on the general product, these sites can correspond to different pixels on the high-resolution product from the dual-scale retrieval results. We call these ground sites “dense points”. If the generated high-resolution product can keep high consistency with the $PM_{2.5}$ values of these dense points, it means that the generated detail information in the high-resolution map can effectively capture the real fine-scale $PM_{2.5}$ variations. This process is explained in Fig. 3. When conducting the 10-fold cross-validation, the Pearson correlation coefficient (r) between the $PM_{2.5}$ concentration of these dense points and the corresponding grids of the produced $PM_{2.5}$ product was calculated as the indicator.

3. Results

3.1. Model performance

To fully verify the performance of the dual-scale retrieval method, we selected the traditional single-scale retrieval method for a comparison, which can be expressed as:

$$PM_{2.5\_S} = f(lat, lon, AOD, TMP, PS, SH, UWS, VWS, LCL, OME, PR, PBLH, LC, DEM, [month, TT_{PM2.5}])$$

where $PM_{2.5\_S}$ represents the $PM_{2.5}$ retrieved from the single-scale method, and *f()* represents the retrieval models, which are the same as the models used for the dual-scale retrieval method. Specially, for GWR model, *lat* and *lon* should be removed from the input, as has been described in Section 2.3.1. It should be noted that the $PM_{2.5\_S}$ product is at the resolution of 0.1°×0.1°; that is to say, it is nearly 30 times lower than the resolution of the dual-scale retrieval results, i.e., $PM_{2.5\_H}$.

The model fitting and validation performance are shown in Table 1.

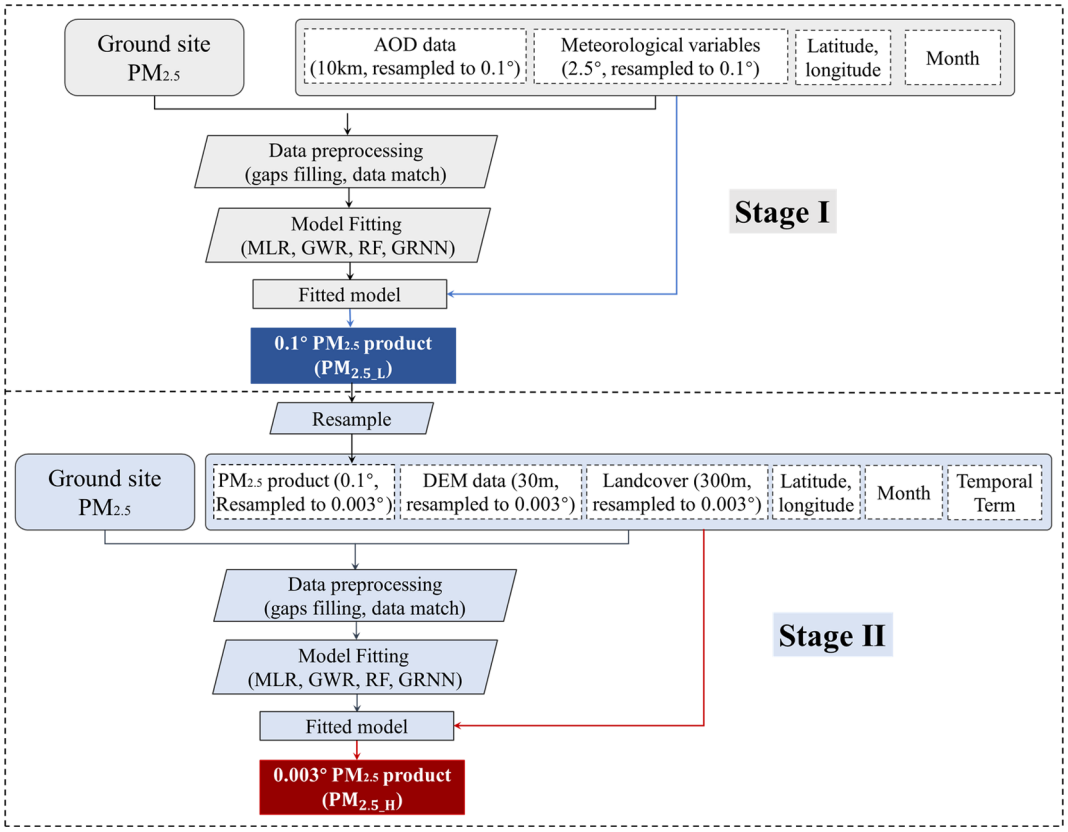

Fig. 2. Flow chart of the dual-retrieval method. The upper (gray) part represents the first stage, and the lower (light blue) part represents the second stage.

We can find that, for most cases, the proposed dual-scale retrieval approach shows an improvement over the traditional single-scale retrieval approach. Specifically, the cross-validation R^2 improves by 0.01, 0.06, 0.05, and 0.04 for the annual MLR, GWR, RF, and GRNN models, respectively, and improves by 0.01, 0.02, 0.07, and 0.04 for the daily MLR, GWR, RF and GRNN models, respectively. For annual model, GWR performs best, with the fitting R^2 and cross-validation R^2 reaching 0.86 and 0.85, respectively. Then come the GRNN and RF model, with the fitting R^2 being 0.74 for GRNN and 0.73 for RF, and the cross-validation R^2 being 0.73 for GRNN and 0.72 for RF. For daily model, RF shows the best performance with the cross-validation R^2 reaching 0.72. GWR and GRNN follow. The MLR model shows the worst performance among the four models at both modeling scales (daily and annual), with a cross-validation R^2 of 0.67 for annual model and 0.62 for daily model. This proves that simple linear regression may not be able to describe the complex relationship between $PM_{2.5}$ and the multiple influencing factors at different resolutions well. For all the results of dual-scale retrieval, the fitting R^2 and CV R^2 were very close, with a difference no more than 0.02, which is a very small difference and proved that overfitting problem didn't exist in our dual-scale retrieval model. In the GWR-based single-scale model, the overfitting problem can exist with the difference between fitting and CV R^2 reach 0.06 for the annual model and 0.05 for daily model. Dual-scale retrieval can reduce the overfitting problem for the GWR-based model.

We also show scatter plots of the cross-validation results. Fig. 4 shows the results for annual modeling. Apart from having the highest

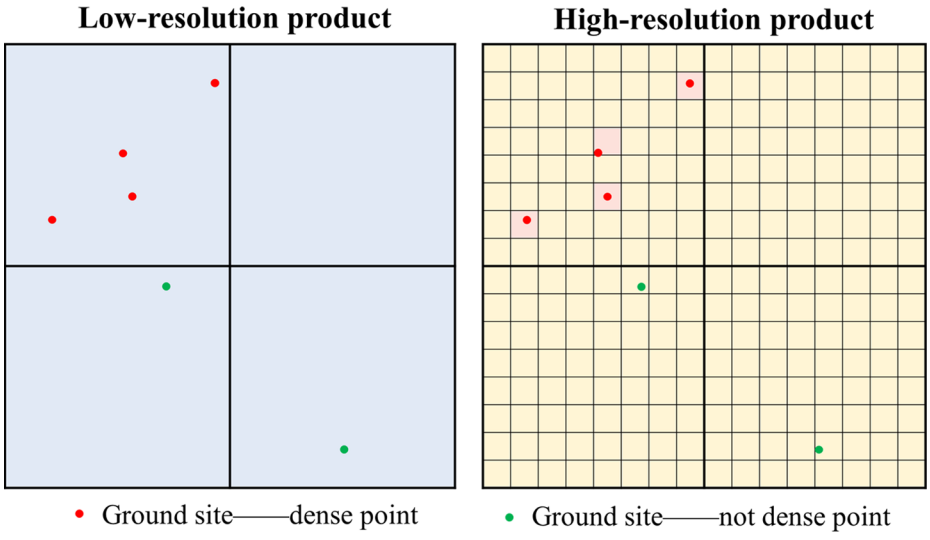

Fig. 3. Schematic for the dense-point validation. The light blue square represents the low-resolution product and the light orange square represents the high-resolution product. Each grid represents one pixel. The points (including green and red points) represent the ground sites, while the red points are the dense points. The pink grids are the corresponding pixels to the dense points.

Table 1
The model fitting and cross-validation results. Fitting R^2 is the R^2 score for the model fitting, and CV R^2 represent the R^2 score for the cross-validation. S I and S II represent the first and second stage of dual-scale retrieval respectively. Annual and daily refer to the annual modeling and daily modeling results.

			MLR		GWR		RF		GRNN	
			Fitting R^2	CV R^2	Fitting R^2	CV R^2	Fitting R^2	CV R^2	Fitting R^2	CV R^2
Annual	**Dual-scale**	**S I**	0.59	0.58	0.84	0.78	0.74	0.72	0.61	0.60
		S II	0.68	0.67	0.86	0.85	0.73	0.72	0.74	0.73
	Single-scale		0.67	0.66	0.85	0.79	0.68	0.67	0.70	0.69
Daily	**Dual-scale**	**S I**	0.33	0.33	0.56	0.52	0.58	0.56	0.54	0.52
		S II	0.62	0.62	0.70	0.69	0.74	0.72	0.68	0.66
	Single-scale		0.61	0.61	0.72	0.67	0.67	0.65	0.64	0.62

cross-validation R^2 score, the fitting line of the scatters of the GWR model is also the closest to the 1:1 line, with the slope equaling 0.85, indicating a small bias. As for the other three retrieval models, the slopes for the fitting lines are 0.67, 0.64, and 0.68 respectively. The scatter shape for RF model can be a little discontinuous, which indicate that the mapping results may be unsmooth. Then Fig. 5 shows the results for daily modeling. The scatters of RF and GWR model were more compact and the fitting lines were closer to the 1:1 line than other regression models, with the slopes equaling 0.68. All the slopes in Fig. 4 and Fig. 5 are smaller than 1, which means that overestimation for lightly polluted regions and underestimation for highly polluted regions exist. This is a common problem for $PM_{2.5}$ retrieval research (He and Huang, 2018; Xue et al., 2019).

The results of the dense-point cross-validation are displayed in Fig. 6 and Table 2. Fig. 6 shows the specific process for dense-point cross-validation, taking the retrieval results of annual GWR-based model in Guangzhou as an example. The two upper images are the results of the single-scale and dual-scale retrieval in Guangzhou. We can clearly see that the result of the single-scale retrieval is very coarse, and there are many sites which have different $PM_{2.5}$ concentration values located in the same pixel (marked by the black rectangles). The detailed spatial variations are covered up by the coarse pixels. In contrast, the result of the dual-scale retrieval is much smoother, and contain more detailed information about the spatial variations. The ground monitoring sites also correspond to different pixels. Compared with the traditional single-scale retrieval approach, the dual-scale retrieval brings about a more than 30-times improvement on resolution, making the $PM_{2.5}$ mapping at the city level much smoother and containing rich details. For a quantitative evaluation of the accuracy of the detail information built by the dual-scale retrieval approach, we calculated the correlation coefficient between the $PM_{2.5}$ concentration values of these dense points and the corresponding pixels for single- and dual-scale retrieval results in Guangzhou. The results are listed in the lower part of Fig. 6. The correlation coefficient is 0.71 for the dual-scale retrieval,

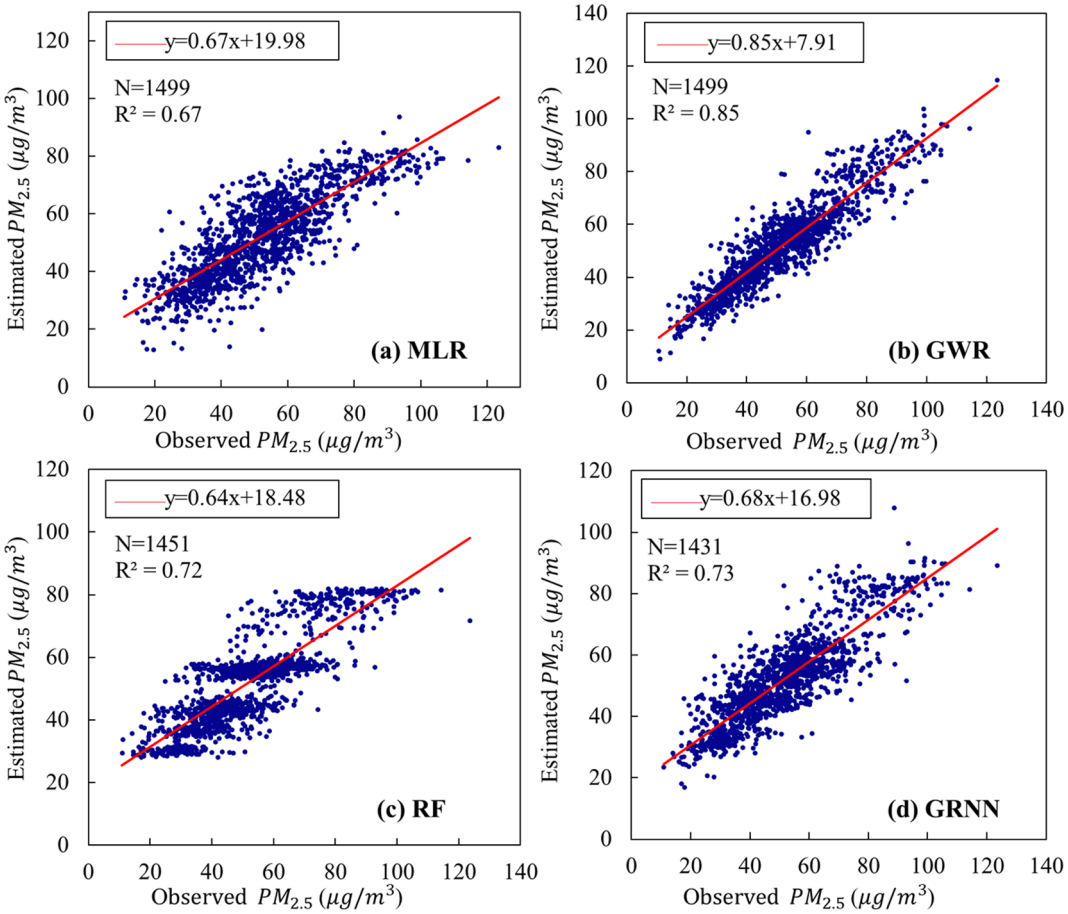

Fig. 4. The scatter plots for the cross-validation results of the four annual retrieval models. (a) MLR-; (b) GWR-; (c) RF-; (d) GRNN-based dual-scale retrieval at annual scale. The red lines are the fitted lines for the scatters. N is the sample number.

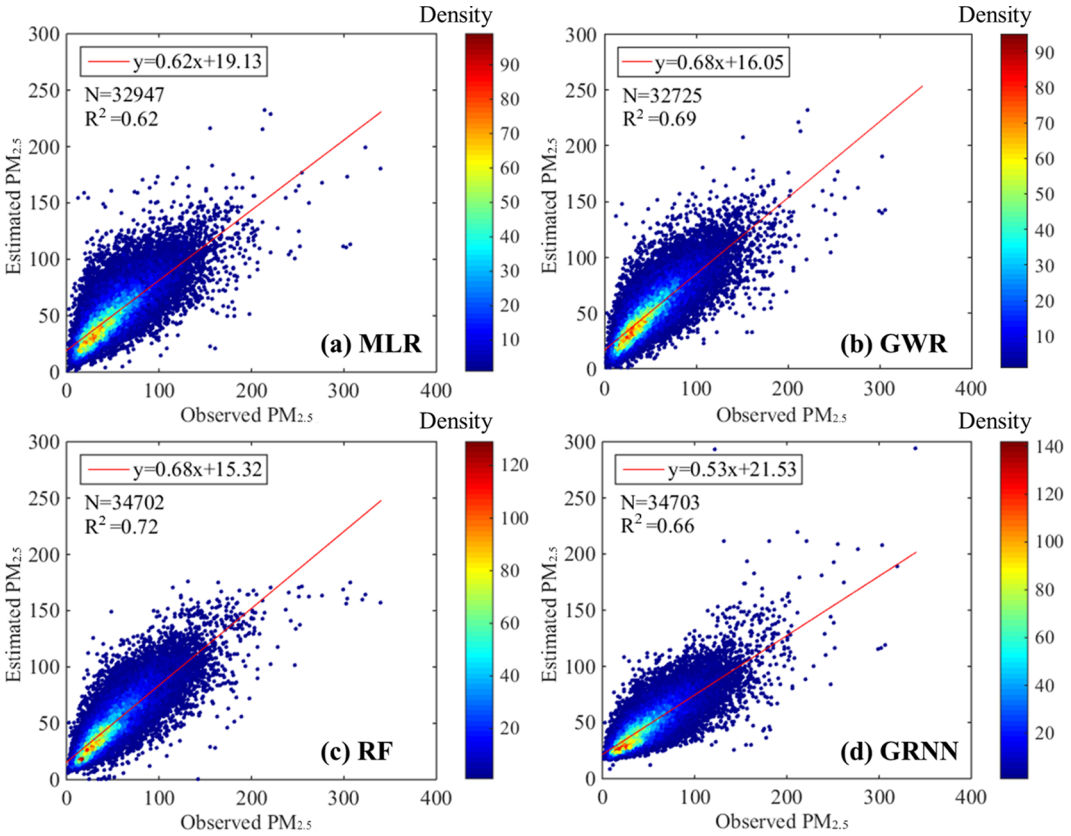

Fig. 5. The scatter plots for the cross-validation results of the four daily retrieval models. (a) MLR-; (b) GWR-; (c) RF-; (d) GRNN-based dual-scale retrieval at daily scale. The red lines are the fitted lines for the scatters. N is the sample number. The color for the points represents the point density.

and for single-scale retrieval, the value is just 0.50. This means that, with the resolution of the retrieval result improved from 0.1° to 0.003°, the detail information is built and correctly incorporated in the dual-scale retrieval results.

Table 2 displays the results of dense-point cross-validation for annual modeling and daily modeling using the four different regression models. The predicted values at these dense points were calculated at each fold of the cross-validation. Both dense-points cross-validation results for single- and dual-scale retrieval are listed for a comparison. We can see that the dual-scale retrieval has a higher dense-point cross-validation r value under all cases. For MLR, GWR, GRNN and RF, the r values improve 0.01, 0.05, 0.02, and 0.03 for annual modeling, and meanwhile, improve 0.01, 0.02, 0.04, and 0.02 for daily modeling. The scatter plots for dense-point validation results can be found in the supplementary material (Fig. S4 and Fig. S5). We found that dual-scale also outperforms single-scale model in terms of scatter plots, with the slopes closer to 1 and the intercepts closer to 0 than single-scale model.

3.2. $PM_{2.5}$ mapping at the sub-km level

The proposed dual-scale retrieval method can not only acquire a higher prediction accuracy, but it can also generate a final product with a higher spatial resolution. We selected several typical cities in China and drew the $PM_{2.5}$ concentration distribution map at the resolution of 0.003° using the proposed method. For a comparison, the mapping results of both the single-scale and dual-scale retrieval methods are displayed. Fig. 7 displays the results of the annual models. We can clearly see that the $PM_{2.5}$ mapping results of the dual-scale retrieval have similar spatially varying trends to the results of the single-scale retrieval. In addition, more detailed information can be captured by the dual-scale retrieval than the single-scale retrieval, and the mapping results are more continuous and smoother. The results for daily modeling were displayed in Fig. S6 and Fig. S7. Daily retrieval results suffer from serious data missing problem, but we can still find that the results of dual-scale retrieval are smoother in spatial variations than the results of single-scale retrieval. The annual distributions averaged from daily estimates then show similar results to the annual model outputs (Fig. S7). This indicates that the dual-scale retrieval approach can greatly improve the mapping quality.

Although the proposed method has a strong expression ability of spatial detail under all the retrieval models and at both modeling scales (daily modeling and annual modeling), the retrieved values and mapping quality vary under the different retrieval models. In terms of the retrieved values, MLR and GRNN tend to acquire higher $PM_{2.5}$ concentrations than GWR and RF. RF shows the worst mapping performance with the mapping results showing blocking and stratification phenomena (consistent with the scatter shape of cross-validation in Fig. 4(c)), although RF has a quite satisfying performance in the quantitative evaluation. The bad mapping quality of RF in retrieval problem has also been found by other researches in their work, and it was reported that the feature of RF algorithm and the type of input variables contribute to the bad mapping quality together (Yuan et al., 2019; Zhao et al., 2017; Shi et al., 2015). For the other three retrieval models, the $PM_{2.5}$ concentration maps are spatially continuous and show a high mapping quality. For the five cities with different climates, topographies, and pollution degrees, the proposed method shows a good stability in mapping quality. Overall, the retrieval experiments under four retrieval models in five different cities prove that the dual-scale retrieval method is a robust retrieval approach that has the potential to be applied to multifarious regions.

For a clearer display of the details of the dual-scale retrieval results, we selected two typical regions in Wuhan and used the annual retrieval results to show the spatial details. The two regions are marked with red rectangles in the GWR-based dual-scale retrieval results for Wuhan in

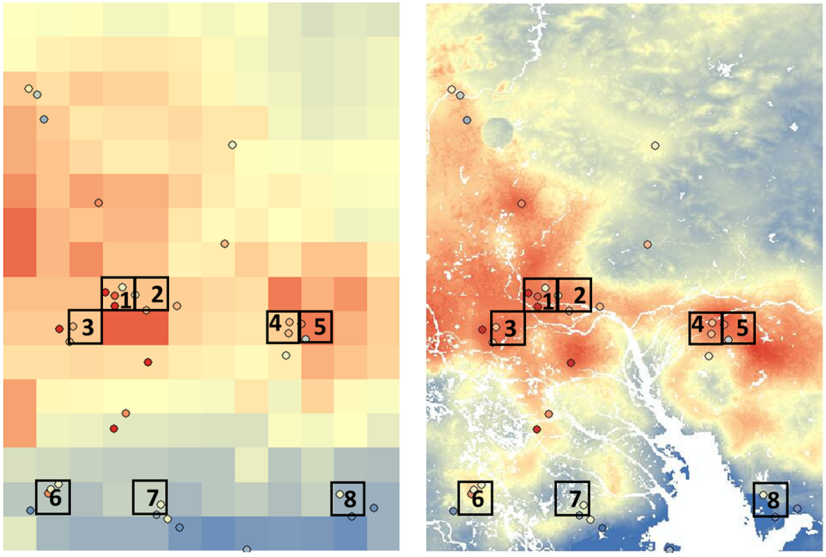

Grid	Point	LR value	S value	HR value	Grid	Point	LR value	S value	HR value
1	1-1	37.10	34.69	39.35	5	5-1	40.34	39.48	41.37
	1-2	37.10	41.42	40.71		5-2	40.34	33.78	39.33
	1-3	37.10	39.91	40.42	6	6-1	30.81	34.09	35.38
	1-4	37.10	42.56	40.34		6-2	30.81	34.73	35.43
2	2-1	37.10	35.73	40.05		6-3	30.81	39.46	35.86
	2-2	37.10	37.29	38.94	7	7-1	31.57	34.19	32.51
3	3-1	36.97	37.50	40.07		7-2	31.57	32.27	32.29
	3-2	36.97	38.01	40.79	8	8-1	30.39	35.04	32.63
4	4-1	36.71	37.57	40.99		8-2	30.39	30.44	31.98
	4-2	36.71	37.33	40.18			r_{SL}=0.50		r_{SH}=0.71

Fig. 6. The dense-point validation results: an example of the retrieved results of annual GWR model for Guangzhou. The black rectangles are the grids where the dense points are located. These grids are numbered from top to bottom, left to right. Points in the grids are also numbered by grid number-*, from top to bottom, left to right. The LR and HR values are the estimated $PM_{2.5}$ values of the single-scale and dual-scale retrieval results, respectively, and the S value is the ground site $PM_{2.5}$ value. r_{SH} (r_{SL}) stands for the Pearson correlation coefficient between the dense-points-measured $PM_{2.5}$ and the dual-scale (single-scale)-retrieved $PM_{2.5}$ concentration.

Table 2
The dense-point cross-validation results of single- and dual-scale retrieval for the four regression models. Annual and daily represent the results for annual modeling and daily modeling.

		MLR	GWR	RF	GRNN
Annual	**Single-scale**	0.82	0.88	0.82	0.83
	Dual-scale	0.83	0.93	0.84	0.86
Daily	**Single-scale**	0.78	0.81	0.80	0.79
	Dual-scale	0.79	0.83	0.84	0.81

Fig. 7. As shown in Fig. 8, these regions can only be represented by less than 2 pixels in the results of the single-scale retrieval, but in the results of the dual-scale retrieval, there is rich detail information, which can detect the locations of some typical emission sources and green belts correctly. For example, in the results for East Lake, the regions marked by red polygons in Fig. 8(c) are all mature green belt areas in Wuhan, and in Fig. 8(b), they all show lower $PM_{2.5}$ concentrations than the adjacent regions. Thus, the protective effect of urban green belts on air pollution can be detected in our results. Furthermore, in the results for Qingshan Harbor, which is an industrial area of Wuhan, the $PM_{2.5}$ emissions from factories can be detected. In Fig. 8(f), the regions marked by the red polygons are mainly dense factories, and we can even see the big chimney in the yellow box. Correspondingly, these regions come with higher $PM_{2.5}$ pollution levels, as shown in Fig. 8(e).

Finally, the GWR-based dual-scale retrieval model has also been used for 2013 and 2014 for the high-resolution $PM_{2.5}$ mapping at corresponding years. The specific model evaluation and mapping results can be found in the supplementary material Text 4.

4. Discussion

4.1. Different regression models for different scales

In the experiments part, for a fair comparison with single-scale retrieval, we set the regression models for the two stages the same. But in fact, the combination of different regression models at different stages may worth exploration. Therefore, we make a further experiment to find out the performance. We took the annual modeling as an example and adopted different regression models in the two stages. The results are listed in Table 3, the combinations with CV R^2 larger than 0.72 are highlighted in bold font. Generally, the combination of 'GWR + GWR' shows the best performance. Besides, introduction of GWR to the model (no matter at which scale) can improve the model performance. For example, with the first scale regression model set to be MLR (see the first two rows in Table 3), using GWR as the second-scale regression model can improve the model performance a lot, with the CV R^2 improves by 0.11 compared with MLR as regression model of second scale.

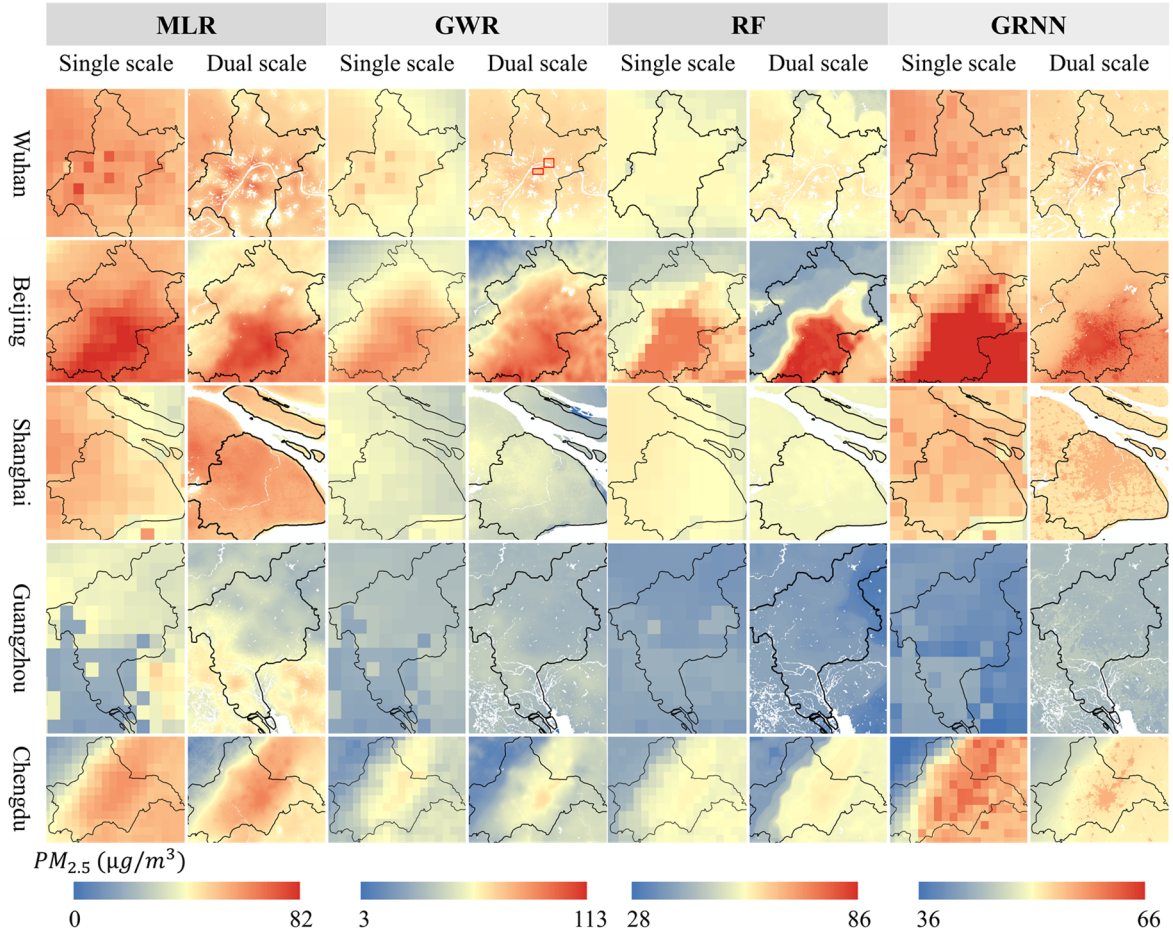

Fig. 7. The $PM_{2.5}$ concentration distribution maps for 2015 in five typical cities using four different annual retrieval models. The results of both the single- and dual-scale retrieval are displayed for a comparison. The white areas in the dual-scale retrieval results are the watersheds, and the black lines are the administrative boundaries for the cities.

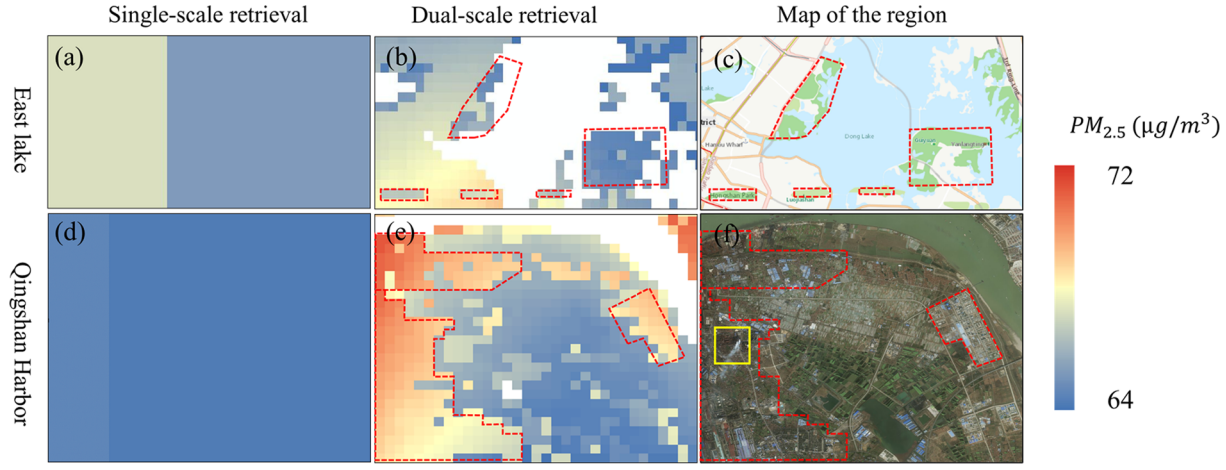

Fig. 8. The annual GWR-based single- and dual-scale retrieval results for East Lake and Qingshan Harbor in Wuhan. The first row are the results for the East Lake region, and the second row are the results for Qingshan Harbor. (a) and (d) are the single-scale retrieval results; (b) and (e) are the dual-scale retrieval results; and (c) and (f) are the topographic and satellite maps.

Using RF and GRNN as the second-scale retrieval model can also improve the model performance compared with the 'MLR + MLR' combination.

4.2. Comparison of four regression models

Under the dual-scale retrieval framework, the performance of the four retrieval models varies a lot, which is worth further discussion.

Firstly, when conducting the retrieval using the MLR model, the dual-scale retrieval did not improve much when compared to the single-scale retrieval, the fitting R^2 and cross-validation R^2 only increased by 0.01 for both annual and daily modeling (Table 1). We think this may be explainable. A key point for retrieval is to accurately describe the relationships between $PM_{2.5}$ and its impacting factors. The relationships

Table 3
The performances for models with different regression models at different scales.

			Model for scale 2			
			MLR	GWR	RF	GRNN
Model for scale 1	MLR	Fitting R2	0.678	**0.839**	0.722	0.724
		CV R2	0.673	**0.783**	0.706	0.707
	GWR	Fitting R2	**0.827**	**0.855**	**0.817**	**0.742**
		CV R2	**0.826**	**0.848**	**0.808**	**0.730**
	RF	Fitting R2	0.686	**0.832**	0.733	0.704
		CV R2	0.677	**0.753**	0.716	0.694
	GRNN	Fitting R2	0.701	**0.844**	0.709	**0.743**
		CV R2	0.695	**0.778**	0.698	**0.725**

are usually complex and nonlinear and therefore cannot be well captured by MLR model. Therefore, even though the retrieval approach was optimized, the MLR model cannot display it well due to its poor ability to describe complex relationships.

Secondly, the best-performing models change as the modeling scale changes. The experiments of annual modeling showed that GWR obtained the best performance, transcending the performance of the ML-based models. In contrast, RF model got the highest quantitative evaluation score in daily modeling experiments. We believe that there are two main reasons for this phenomenon. Firstly, when we built the model at annual scale, the temporal information was not considered, so only spatial predictions were made. GWR is a model known for considering spatial heterogeneity and perform satisfactorily for spatial predictions; hence, it may show good performance in annual modeling. Meanwhile, daily modeling contains large temporal information, which is not well considered in GWR model. In this case, machine learning models show their strong learning ability. Secondly, the number of samples used for the annual model training was at around 1430. But for daily model, the number is more than 30 thousand. The small amount of training samples limits the data mining ability of the machine learning algorithms in annual modeling, therefore, GWR can perform better than the ML-based models. This remind us that, although the ML-based model can achieve a decent performance in many cases, this may not apply for all situations. For example, as a data-driven algorithm, ML may not be suitable for studies without massive data. In addition, some of the traditional models have potential that is worth deeper exploration.

4.3. Why dual-scale retrieval?

In fact, if we want to achieve the high-resolution $PM_{2.5}$ mapping without extra high-resolution AOD as input, there is another simple and direct solution–we can resample all the input data into 0.003° and then conduct the single-scale retrieval (single-scale retrieval at 0.003°), why should we propose the dual-scale retrieval? Resample from low resolution to high resolution (downscaling) is usually accompanied with large uncertainties. Compared with resampling all the data to 0.1°, resampling all the data to 0.003° can bring larger uncertainties with little useful information introduced, which can usually result in the decrease of model performance (the evidence from experiments can be found in supplementary material Text 5, Fig. S11 and Table S5). Therefore, if we want to improve the model performance while improving the resolution of retrieved results, we need to decrease the downscaling uncertainties or improve the information extraction ability. Dual-scale retrieval aimed at improving the information extraction ability. Through splitting the retrieval process into two stages and using the dominant variables of this scale for retrieval at corresponding scale, the information extraction ability may have been improved because all the predictors are predicting at the scale they dominate. Instead, in the single-scale model, all the predictors are mixed, so none of them can predict at their best scales due to the bad inter-disturbance. We believe, that's the reason for the improvement of dual-scale retrieval compared with single-scale retrieval.

4.4. Limitations and future work

Although the proposed approach can achieve a great improvement in resolution and retrieval accuracy, the number of variables with a high resolution to help with the detail construction was small. In the future, we would like to explore and introduce more variables with a high resolution. The introduction of multisource high-resolution data may be able to describe the detailed variations of $PM_{2.5}$ concentration in a better way. Furthermore, the experiments on daily modeling showed that the daily retrieval results suffer from serious data missing problem, which mainly attribute to the data missing of AOD product. In the future, we would like to consider some gap filling approaches (Wang et al., 2019b) for AOD data preprocessing, to improve the coverage of daily retrieval results. In addition, in this study, we only tested the performance of dual-scale retrieval. Retrieval using more scales, i.e., multi-scale retrieval, was not attempted, for fear that the repeat resampling of the low-resolution product may bring large uncertainties, thus decreasing the model accuracy and the generalization ability of the model. In fact, in the future, if we can obtain enough data at multiple resolutions, it will be worth trying to expand the dual-scale retrieval to multi-scale retrieval, to obtain a $PM_{2.5}$ product at a higher resolution than 0.003°. Finally, the proposed dual-scale retrieval method can not only be used for $PM_{2.5}$ concentration mapping, but it also has great potential for the production of other quantitative remote sensing products, such as soil moisture and vegetation parameters. With both the accuracy and resolution improved, the application value of the quantitative remote sensing products could be greatly improved.

5. Conclusions

The traditional satellite-based $PM_{2.5}$ retrieval method achieves $PM_{2.5}$ mapping at the resolution of the AOD, with all the auxiliary variables resampled to the resolution of the AOD, regardless of the fact that the variables with a higher resolution than the AOD may contain important detail information for capturing the spatial variations of $PM_{2.5}$ at a fine scale. In this paper, we have proposed a dual-scale retrieval method to make better use of the information contained within the variables with different resolutions. Variables with a low resolution are used for the first-scale retrieval at a coarse scale, and then the variables at a higher resolution are used for the retrieval at a fine scale. As the connection between the retrievals at the two scales, the $PM_{2.5}$ product of the first stage is downscaled and input into the model in the second stage. The results of the four regression models, i.e., MLR, GWR, RF, and GRNN, at two different temporal modeling scales, i.e., annual modeling and daily modeling, showed that the dual-scale retrieval can achieve a higher estimation accuracy, and can map the $PM_{2.5}$ concentration at a higher resolution than the single-scale retrieval. Fine-scale spatial variations can be constructed correctly in the dual-scale retrieval, which is a great improvement for $PM_{2.5}$ mapping at the city scale. To date, most of the studies researching $PM_{2.5}$ mapping at the sub-kilometer scale have concentrated on the use of high-resolution AOD products. In this study, we achieved the mapping of $PM_{2.5}$ concentration at sub-kilometer resolution without high-resolution AOD as input, by changing the retrieval approach. Dual-scale retrieval solves the problem of high-resolution AOD products often being difficult to obtain, and make the high-resolution $PM_{2.5}$ mapping at large extent (national to global) more easily achievable.

Declaration of Competing Interest

The authors declared that there is no conflict of interest.

Acknowledgments

This work was supported by the Strategic Priority Research Program of the Chinese Academy of Sciences (No. XDA19090104), the National Natural Science Foundation of China (No. 41922008), the Fundamental Research Funds for the Central Universities of Wuhan Univeristy (No. 2042019kf0213), and the Science and Technology Major Project of Hubei Province (No. 2019AAA046). We would also like to thank the $PM_{2.5}$ data providers of the China National Environmental Monitoring Center (CNEMC). The MODIS AOD data were obtained from the NASA Langley Research Center Atmospheric Science Data Center (ASDC). The MERRA-2 reanalysis data were provided by NASA's Goddard Earth Sciences Data and Information Services Center. Finally, we would also like to thank the ESA team for providing the land-cover data.

Appendix A. Supplementary material

Supplementary data to this article can be found online at https://doi.org/10.1016/j.isprsjprs.2020.05.018.

References

Beloconi, A., Kamarianakis, Y., Chrysoulakis, N., 2016. Estimating urban PM10 and $PM_{2.5}$ concentrations, based on synergistic MERIS/AATSR aerosol observations, land cover and morphology data. Remote Sens. Environ. 172, 148–164.

Bi, J., Belle, J.H., Wang, Y., Lyapustin, A.I., Wildani, A., Liu, Y., 2019. Impacts of snow and cloud covers on satellite-derived $PM_{2.5}$ levels. Remote Sens. Environ. 221, 665–674.

Bottenberg, R.A., Ward, J.H., 1963. Applied multiple linear regression (Vol. 63, No. 6). 6570th Personnel Research Laboratory, Aerospace Medical Division. Air Force Systems Command, Lackland Air Force Base.

Boys, B.L., Martin, R.V., van Donkelaar, A., MacDonell, R.J., Hsu, N.C., Cooper, M.J., Yantosca, R.M., Lu, Z., Streets, D.G., Zhang, Q., Wang, S.W., 2014. Fifteen-year global time series of satellite-derived fine particulate matter. Environ. Sci. Technol. 48, 11109–11118.

Breiman, L., 2001. Random Forest. Machine Learning 45, 5–32.

Brunsdon, C., Stewart Fotheringham, A., Charlton, M.E., 1996. Geographically Weighted Regression A Method for Exploring. Spatial Nonstationarity. Geographical Analysis.

Cao, C., Lee, X., Liu, S., Schultz, N., Xiao, W., Zhang, M., Zhao, L., 2016. Urban heat islands in China enhanced by haze pollution. Nat. Commun. 7, 12509.

Ceca, L.S.D., Ferreyra, M.F.G., Lyapustin, A., Chudnovsky, A., Otero, L., Carreras, H., Barnaba, F., 2018. Satellite-based view of the aerosol spatial and temporal variability in the Cordoba region (Argentina) using over ten years of high-resolution data. ISPRS J. Photogram. Remote Sensing : Official Publ. Int. Soc. Photogram. Remote Sensing 145, 250–267.

Chen, G., Li, S., Knibbs, L.D., Hamm, N.A.S., Cao, W., Li, T., Guo, J., Ren, H., Abramson, M.J., Guo, Y., 2018. A machine learning method to estimate $PM_{2.5}$ concentrations across China with remote sensing, meteorological and land use information. Sci. Total Environ. 636, 52–60.

Chen, R., Yin, P., Meng, X., Wang, L., Liu, C., Niu, Y., Liu, Y., Liu, J., Qi, J., You, J., Kan, H., Zhou, M., 2019. Associations between Coarse particulate matter air pollution and cause-specific mortality: a nationwide analysis in 272 Chinese cities. Environ. Health Perspect. 127, 17008.

Chen, Z., Xie, X., Cai, J., Chen, D., Gao, B., He, B., Cheng, N., Xu, B., 2017. Understanding meteorological influences on $PM_{2.5}$ concentrations across China: a temporal and spatial perspective. Atmos. Chem. Phys. Discussions 1–30.

Chung, C. E. (2012). Aerosol direct radiative forcing: a review. Atmospheric Aerosols—Regional Characteristics—Chemistry and Physics; Abdul-Razzak, H., Ed, 379-394.

Cigizoglu, H.K., Alp, M., 2006. Generalized regression neural network in modelling river sediment yield. Adv. Eng. Softw. 37, 63–68.

de Hoogh, K., Heritier, H., Stafoggia, M., Kunzli, N., Kloog, I., 2018. Modelling daily $PM_{2.5}$ concentrations at high spatio-temporal resolution across Switzerland. Environ. Pollut. 233, 1147–1154.

Guo, J.-P., Zhang, X.-Y., Che, H.-Z., Gong, S.-L., An, X., Cao, C.-X., Guang, J., Zhang, H., Wang, Y.-Q., Zhang, X.-C., Xue, M., Li, X.-W., 2009. Correlation between PM concentrations and aerosol optical depth in eastern China. Atmos. Environ. 43, 5876–5886.

Guo, Y., Tang, Q., Gong, D.-Y., Zhang, Z., 2017. Estimating ground-level PM 2.5 concentrations in Beijing using a satellite-based geographically and temporally weighted regression model. Remote Sens. Environ. 198, 140–149.

Gupta, P., Christopher, S.A., Wang, J., Gehrig, R., Lee, Y., Kumar, N., 2006. Satellite remote sensing of particulate matter and air quality assessment over global cities. Atmos. Environ. 40, 5880–5892.

He, Q., Geng, F., Li, C., Yang, S., Wang, Y., Mu, H., Zhou, G., Liu, X., Gao, W., Cheng, T., Wu, Z., 2018. Long-term characteristics of satellite-based $PM_{2.5}$ over East China. Sci. Total Environ. 612, 1417–1423.

He, Q., Huang, B., 2018. Satellite-based mapping of daily high-resolution ground PM 2.5 in China via space-time regression modeling. Remote Sens. Environ. 206, 72–83.

Ho, H.C., Wong, M.S., Yang, L., Chan, T.C., Bilal, M., 2018. Influences of socioeconomic vulnerability and intra-urban air pollution exposure on short-term mortality during extreme dust events. Environ. Pollut. 235, 155–162.

Hu, X., Belle, J.H., Meng, X., Wildani, A., Waller, L.A., Strickland, M.J., Liu, Y., 2017. Estimating $PM_{2.5}$ Concentrations in the Conterminous United States Using the Random Forest Approach. Environ. Sci. Technol. 51, 6936–6944.

Hu, X., Waller, L.A., Lyapustin, A., Wang, Y., Al-Hamdan, M.Z., Crosson, W.L., Estes, M.G., Estes, S.M., Quattrochi, D.A., Puttaswamy, S.J., Liu, Y., 2014. Estimating ground-level $PM_{2.5}$ concentrations in the Southeastern United States using MAIAC AOD retrievals and a two-stage model. Remote Sens. Environ. 140, 220–232.

Huang, K., Xiao, Q., Meng, X., Geng, G., Wang, Y., Lyapustin, A., Gu, D., Liu, Y., 2018. Predicting monthly high-resolution $PM_{2.5}$ concentrations with random forest model in the North China Plain. Environ. Pollut. 242, 675–683.

J. Lelieveld, J.S.E., M. Fnais, D. Giannadaki & A. Pozzer, 2015. The contribution of outdoor air pollution sources to premature mortality on a global scale. nature Geoscience.

Jackson, J. M., Liu, H., Laszlo, I., Kondragunta, S., Remer, L. A., Huang, J., and Huang, H. -C., 2013, Suomi-NPP VIIRS aerosol algorithms and data products, J. Geophys. Res. Atmos., 118, 12,673– 12,689.

Jiang, M., Sun, W., Yang, G., Zhang, D., 2017. Modelling seasonal GWR of Daily $PM_{2.5}$ with proper auxiliary variables for the yangtze river delta. Remote Sensing 9, 346.

Jung, Chau-Ren, Hwang, Bing-Fang, Chen, Wei-Ting, 2018. Incorporating long-term satellite-based aerosol optical depth, localized land use data, and meteorological variables to estimate ground-level $PM_{2.5}$ concentrations in Taiwan from 2005 to 2015. Environ. Pollut. 237, 1000–1010. https://doi.org/10.1016/j.envpol.2017.11.016.

Levy, R.C., Mattoo, S., Munchak, L.A., Remer, L.A., Sayer, A.M., Hsu, N.C., 2013. The Collection 6 MODIS aerosol products over land and ocean. Atmos. Meas. Tech. Discuss. 6, 159–259.

Levy, R.C., Remer, L.A., Mattoo, S., Vermote, E.F., Kaufman, Y.J., 2007. Second-generation operational algorithm: Retrieval of aerosol properties over land from inversion of Moderate Resolution Imaging Spectroradiometer spectral reflectance. J. Geophys. Res.: Atmosph. 112.

Li, G., Fang, C., Wang, S., Sun, S., 2016. The Effect of Economic Growth, Urbanization, and Industrialization on Fine Particulate Matter ($PM_{2.5}$) Concentrations in China. Environ. Sci. Technol. 50, 11452–11459.

Li, T., Shen, H., Yuan, Q., Zhang, X., Zhang, L., 2017a. Estimating Ground-Level PM2.5 by Fusing Satellite and Station Observations: A Geo-Intelligent Deep Learning Approach. Geophysical Research Letters 44, 11,985-911,993.

Li, T., Shen, H., Zeng, C., Yuan, Q., Zhang, L., 2017b. Point-surface fusion of station measurements and satellite observations for mapping PM 2.5 distribution in China: Methods and assessment. Atmos. Environ. 152, 477–489.

Liu, N., Zou, B., Feng, H., Tang, Y., Liang, Y., 2019. Evaluation and comparison of MAIAC, DT and DB aerosol products over China. Atmos. Chem. Phys. Discuss. 1–34.

Ma, Z., Hu, X., Huang, L., Bi, J., Liu, Y., 2014. Estimating ground-level $PM_{2.5}$ in China using satellite remote sensing. Environ. Sci. Technol. 48, 7436–7444.

Ma, Z., Hu, X., Sayer, A.M., Levy, R., Zhang, Q., Xue, Y., Tong, S., Bi, J., Huang, L., Liu, Y., 2016. Satellite-Based Spatiotemporal Trends in $PM_{2.5}$ Concentrations: China, 2004–2013. Environ. Health Perspect. 124, 184–192.

Ning, G., Wang, S., Ma, M., Ni, C., Shang, Z., Wang, J., Li, J., 2018. Characteristics of air pollution in different zones of Sichuan Basin, China. Sci. Total Environ. 612, 975–984.

Peng, J., Loew, A., Merlin, O., Verhoest, N.E., 2017. A review of spatial downscaling of satellite remotely sensed soil moisture. Rev. Geophys. 55 (2), 341–366.

Shi, Y.; Song, L. Spatial Downscaling of Monthly TRMM Precipitation Based on EVI and Other Geospatial Variables Over the Tibetan Plateau From 2001 to 2012. Mt. Res. Dev. 2015, 35.

Stafoggia, M., Bellander, T., Bucci, S., Davoli, M., de Hoogh, K., De' Donato, F., Gariazzo, C., Lyapustin, A., Michelozzi, P., Renzi, M., Scortichini, M., Shtein, A., Viegi, G., Kloog, I., Schwartz, J., 2019. Estimation of daily PM10 and $PM_{2.5}$ concentrations in Italy, 2013–2015, using a spatiotemporal land-use random-forest model. Environ. Int. 124, 170–179.

Tai, A.P.K., Mickley, L.J., Jacob, D.J., 2010. Correlations between fine particulate matter ($PM_{2.5}$) and meteorological variables in the United States: Implications for the sensitivity of $PM_{2.5}$ to climate change. Atmos. Environ. 44, 3976–3984.

Tian, J., Chen, D., 2010. A semi-empirical model for predicting hourly ground-level fine particulate matter ($PM_{2.5}$) concentration in southern Ontario from satellite remote sensing and ground-based meteorological measurements. Remote Sens. Environ. 114, 221–229.

van Donkelaar, A., Martin, R.V., Brauer, M., Kahn, R., Levy, R., Verduzco, C., Villeneuve, P.J., 2010. Global estimates of ambient fine particulate matter concentrations from satellite-based aerosol optical depth: development and application. Environ. Health Perspect. 118, 847–855.

van Donkelaar, A., Martin, R.V., Spurr, R.J., Burnett, R.T., 2015. High-Resolution Satellite-Derived $PM_{2.5}$ from Optimal Estimation and Geographically Weighted Regression over North America. Environ. Sci. Technol. 49, 10482–10491.

Wang, X., Dickinson, R.E., Su, L., Zhou, C., Wang, K., 2017. $PM_{2.5}$ Pollution in China and How It Has Been Exacerbated by Terrain and Meteorological Conditions. Bulletin of the. American Meteorological Society.

Wang, Y., Yuan, Q., Li, T., Shen, H., Zheng, L., Zhang, L., 2019a. Evaluation and comparison of MODIS Collection 6.1 aerosol optical depth against AERONET over regions in China with multifarious underlying surfaces. Atmos. Environ. 200, 280–301.

Wang, Y., Yuan, Q., Li, T., Shen, H., Zheng, L., Zhang, L., 2019b. Large-scale MODIS AOD products recovery: Spatial-temporal hybrid fusion considering aerosol variation mitigation. ISPRS J. Photogramm. Remote Sens. 157, 1–12.

Wei, X., Chang, N.B., Bai, K., Gao, W., 2019. Satellite remote sensing of aerosol optical

depth: advances, challenges, and perspectives. Crit. Rev. Environ. Sci. Technol. 1–86.
Xiao, Q., Wang, Y., Chang, H., Meng, X., Geng, G., Lyapustin, A., Liu, Y., 2017. Full-coverage high-resolution daily $PM_{2.5}$ estimation using MAIAC AOD in the Yangtze River Delta of China. Remote Sens. Environ. 199, 437–446.
Xu, Y., Ho, H.C., Wong, M.S., Deng, C., Shi, Y., Chan, T.C., Knudby, A., 2018. Evaluation of machine learning techniques with multiple remote sensing datasets in estimating monthly concentrations of ground-level $PM_{2.5}$. Environ. Pollut. 242, 1417–1426.
Xue, T., Zheng, Y., Tong, D., Zheng, B., Li, X., Zhu, T., Zhang, Q., 2019. Spatiotemporal continuous estimates of $PM_{2.5}$ concentrations in China, 2000–2016: A machine learning method with inputs from satellites, chemical transport model, and ground observations. Environ. Int. 123, 345–357.
Yang, Q., Yuan, Q., Li, T., Shen, H., Zhang, L., 2017a. The Relationships between $PM_{2.5}$ and Meteorological Factors in China: Seasonal and Regional Variations. Int. J. Environ. Res. Public Health 14, 1510–1528.
Yang, Q., Yuan, Q., Yue, L., Li, T., Shen, H., Zhang, L., 2018. The relationships between $PM_{2.5}$ and AOD in China: About and behind spatiotemporal variations. Environ. Pollut. 248, 526–535.
Yang, X., Zheng, Y., Geng, G., Liu, H., Man, H., Lv, Z., He, K., de Hoogh, K., 2017b. Development of $PM_{2.5}$ and NO2 models in a LUR framework incorporating satellite remote sensing and air quality model data in Pearl River Delta region. China. Environ. Pollut. 226, 143–153.
Yuan, Q., Li, S., Yue, L., Li, T., Shen, H., Zhang, L., 2019. Monitoring the Variation of Vegetation Water Content with Machine Learning Methods: Point-Surface Fusion of MODIS Products and GNSS-IR Observations. Remote Sensing 11, 1440.
Yue, L., Shen, H., Yuan, Q., Zhang, L., 2015. Fusion of multi-scale DEMs using a regularized super-resolution method. Int. J. Geograph. Inform. Sci. 29, 2095–2120.
Yue, L., Shen, H., Zhang, L., Zheng, X., Zhang, F., Yuan, Q., 2017. High-quality seamless DEM generation blending SRTM-1, ASTER GDEM v2 and ICESat/GLAS observations. ISPRS J. Photogramm. Remote Sens. 123, 20–34.
Zhang, T., Zhu, Z., Gong, W., Zhu, Z., Sun, K., Wang, L., Huang, Y., Mao, F., Shen, H., Li, Z., Xu, K., 2018. Estimation of ultrahigh resolution PM 2.5 concentrations in urban areas using 160 m Gaofen-1 AOD retrievals. Remote Sens. Environ. 216, 91–104.
Zhao, X., Jing, W., Zhang, P., 2017. Mapping Fine Spatial Resolution Precipitation from TRMM Precipitation Datasets Using an Ensemble Learning Method and MODIS Optical Products in China. Sustainability 9, 1912.